NUMERICAL SIMULATIONS OF CAVITY RADIUS IN GRANITE: CAVITY BEHAVIOR AS A FUNCTION OF SCALED DEPTH OF BURIAL

Esteban Rougier, Christopher R. Bradley, Howard J. Patton, and Earl. E. Knight.

Los Alamos National Laboratory

Sponsored by the National Nuclear Security Administration

Award No. DE-AC52-06NA25396/LA10-Source-NDD02

ABSTRACT

This paper reports on research activities developed during the first year of this project. The main tasks accomplished and reported in this paper are: a) the development of new computational equation of state (EOS) for granite. One-dimensional calculations using this EOS captures the first principles physics of the near source region and identifies the critical material properties for cavity dynamics. Cavity dynamics are an important consideration for methods that are used to determine accurate estimates of yield under varying emplacement conditions; and b) the extension of the newly developed material models to the analysis of scaled depth of burial and free surface effects in a 2D heterogeneous structure. Efforts in this area are focused on a better understanding of the source stress-cage region as well as free surface Rayleigh and shear wave generation.

A strong motion code for uniform source region structures was used to investigate the dependence of cavity dynamics and final radius on material properties (Young's modulus, shear modulus, gas porosity, overburden, etc.). The material model developed was obtained by taking the PILEDRIVER and the HARDHAT nuclear test events as the main design references. The following aspects of the problem were identified as the driving points when developing the material model: velocity profiles at given stations (near field), source modeling alternatives (iron pill vs. ideal gas vs. Hydses/SESAME), energy partition after the shot, peak velocity and peak displacement attenuation profiles and cavity size as a function of the depth of burial. Previous attempts made with existing material models failed to comply with one or more of the main aspects of the problem. Because of this, a Tillotson type of equation of state with an improved handling of the porosity evolution (crushing and bulking) was implemented, along with a constant yield surface strength model.

The material model developed is used in a set of 2D, axially symmetric simulations aimed at studying the effects of key factors, such as: the variation of the scaled depth of burials (SDoB) and the effects of free surface topography on the cavity dynamics and shear wave generation. A first comparison of the obtained numerical results against the empirical prediction equations shows that the evolution of the calculated final radius of the cavity with the depth of burial is relatively closer to the predictions of Heard's scaling relationship in Mueller and Murphy (1971) than to Denny and Johnson's (1991). Further research needs to be conducted in order to fully understand the cause of the discrepancies between the numerical and the statistical models. Also, the cavity growth, the predicted spall regions, and the seismic radiation associated with the free surface effects are presented.

OBJECTIVES

The NNSA Nuclear Explosion Monitoring Research and Development Roadmaps (2010 these Proceedings) for Ground-Based Systems specifies identification of the sources of waveform signals as an important research and development effort. Source identification is the focus of this project. Understanding the physical basis of seismic wave generation is recognized as the key to advancing our ability to understand and usefully model the explosion source.

The first main objective of the current research is to undertake a series of computer simulations to study the evolution of the cavity radius under different conditions. This phase of computer simulations will employ LANL strong motion codes (CASH) for uniform source region structures (i.e., 1D isotropic velocity models) to investigate the dependence of cavity dynamics and final radius on material properties, such as Young's and shear moduli, gas porosity, overburden (ρgh), regional stresses, etc. The calculations were done using a material having some similarity to the granodiorite that exists at the Democratic People's Republic of Korea (DPRK) test site.

The second main objective of the current work is to perform 2D axially symmetric computer simulations that will introduce 2D sub-surface heterogeneity and free surface topography into the models. Here the focus will be to identify the impact of certain idealized source region structures on the dynamics of cavity growth and on the radiated seismic energy. These 2D structures will be introduced into models of the source region in controlled ways in order to isolate the effects these structures have on the close-in phenomenology and to identify features in the cavity growth and seismic radiation associated with those effects.

RESEARCH ACCOMPLISHED

Modeling an underground nuclear explosion taking into account the propagation of the wave across the elastic region comprises a wide range of physical and thermodynamic phenomena. Four different zones can be identified according to the material behavior. The first zone is called the source region, where the rock and the device material are vaporized due to the huge amount of energy released from the explosion. As the wave created by the explosion propagates outwards the energy dissipates due to mechanical and geometric factors. At a certain range the amount of energy is no longer enough to vaporize the rock but it is sufficient to melt it. This melted region defines the second zone that is called the cavity region. As the wave propagates further the rock material does not melt anymore, but it undergoes plastic deformations. This zone is called the plastic zone. The commonly known *shatter zone* is the first part (closer to the source) of the plastic zone. At a given point located relatively far from the source the material starts behaving elastically, i.e. the elastic zone.

In order to properly account for the wave propagation across all the zones and also for the correct energy deposition in the elastic region of the rock, a series of key constraints concerning each one of the zones must be identified. These constraints are obtained from the available experimental data and are to be employed as design parameters for the purpose of the development of the appropriate material model. In this work, the constraints selected are: velocity and displacement profiles at given stations, energy partition after the shot (for each one of the zones defined above), peak velocity and peak displacement attenuation profiles and cavity size as a function of the depth of burial.

The first part of the modeling effort comprised the development of the material models to be used in the different zones. Regarding the source region, the two most common approaches taken in the past are: iron gas model and the bubble model. The iron gas model assumes that after the explosion an iron gas is formed occupying a relatively small spherical region around the shot point (approximately 1.0 m of radius for a 10 kt source, [Schroeder, 1974]). The initial energy of the explosion is therefore uniformly distributed over this spherical region. The bubble model, on the other hand, considers that the energy of the shot is uniformly distributed over a spherical region with radius equal to the scaled vaporization radius, $r = 2.0\ W^{-1/3}$ [Schroeder, 1974], where W is the yield of the explosion, measured in kilotons and r is the radius of the spherical region in meters. Different materials have been used in the past to model the behavior of the "bubble" or source region. The two most common materials employed for this purpose are: ideal gas [Antoun et al., 2001] with a density equal to the density of the rock under consideration, and a tabular equation of state (EOS), i.e., Hydses type of EOS.

The three approaches for modeling the source region that were described in the previous paragraph were tested during the development of the project. However, none of these source models was able to fulfill simultaneously all of the design constraints mentioned before. The results obtained with the bubble model with an ideal gas provided a very good match with the experimental velocity, displacement, peak velocity and peak displacement attenuation profiles. However, it over predicted the final size of the cavity and also the energy distribution at the end of the simulation was not realistic, i.e. the amount of energy remaining in the source region was only 4% of the total

energy of the explosion. It is worth noting that, depending on the size of the "bubble", the amount of energy needed to vaporize the rock contained inside it ranges from 27% to 35% of the total energy of the explosion. On the other hand, the iron pill and the bubble model with the Hydses granite gave reasonably good results for the final cavity size and for the energy distribution across the zones, but both of them under predicted the velocity, displacement, peak velocity and peak displacement attenuation profiles.

The previously described source model approaches arguably do not fully account for the first principle physics of the shock wave continuum from the cavity expansion all the way up to the final energy deposition in the granite elastic region, i.e. there is a gap between the near source region and the near/far field region dynamics. The importance for future studies of this energy deposition and the proper description of the cavity dynamics combined with the shortcomings of the previously available source modeling approaches generated the necessity of finding a different approach regarding the EOS for the source and for the rest of the granite. Because of this, the Tillotson EOS (Tillotson, 1962) was chosen in an effort to find a bridge for the existing gap between the near source physics phenomena and the near/far field observation points. This EOS is an analytical type and it introduces a dependency on the specific internal energy of the material, which makes it suitable to cover all the zones of the simulation grid. The phase change from solid to vapor is also taken into account. According to the state of the material (expansion or compression) and to the level of specific internal energy the Tillotson EOS divides the *p*-*v* space into four different regions, as shown in Figure 1. The Tillotson EOS utilizes a series of parameters to describe the behavior of the material across the different phases. In this work, the parameter set used was based on Melosh, (1989), with some modifications that were introduced in order to adjust the material model to the lab experiment results. The source modeling was done by coupling this newly implemented EOS with the bubble model.

The material model is completed by combining the EOS of the rock with an appropriate strength model. The strength model describes the resistance of the material to shear deformation. For rock-like materials, the shear strength is dependent on the confinement pressure. The main component of the strength model is the so called "yield surface", which describes how the shear strength changes with the confinement pressure. The yield surface used in the current work was derived from the one proposed by Fossum and Brannon (2004). Some modifications were introduced to the original yield surface in order to match the experimental data from the PILEDRIVER and HARDHAT events. It is worth noting that the shear strength material model utilized in this work considers that the yield surface is constant during the whole simulation, i.e. no effects of strain hardening strain softening, high energy states, etc. are taken into account. A more detailed material model is under development, where all of these effects are to be taken into consideration. The yield surface used in the current work is shown in Figure 2.

The PILEDRIVER and HARDHAT events have been extensively studied in the past and very good matches were obtained between the numerical simulation results and the experimental readings for the velocity, displacement, peak velocity and peak displacement profiles (Antoun et al., 2001; Fossum and Brannon, 2004). However, to the authors' knowledge, a complete analysis of these events, where key near source physics parameters, such as the final cavity size and final energy deposition are included along with the near/far field observational data, i.e. peak attenuation profiles and velocity and displacement profiles has not been reported yet. Because of this, the PILEDRIVER and HARDHAT events were revisited in the current work.

The peak displacement and peak velocity attenuation with the scaled range obtained from the numerical simulations using the material model developed are compared to the data from the experiments corresponding to the PILEDRIVER and HARDHAT nuclear events (Rimer et al., 1990) in Figure 3. The material model provides a remarkable good match for the attenuation of the peak displacements of the HARDHAT event. In the case of the attenuation of the peak velocity, the numerical results over estimate the experimental data for HARDHAT. This could be explained by the fact that in the real world there are several dissipation factors that are not currently being considered in the material model, i.e. weathered material, pre existing cracks and faults, non homogeneous material formations, etc. An interesting feature to be extracted from the graphs presented in Figure 3 is the clear demarcation of the elastic limit, i.e. the point where the material ceases to behave plastically (yielding) to start behaving completely elastically. For the material model developed in this work, this threshold is located at a scaled distance of approximately 200 m / $kt^{1/3}$.

The PILEDRIVER event presents a trend that is shifted with respect to the HARDHAT event, even though both of them were conducted on the same type of material (NTS granite). Further research is being conducted to try to explain the discrepancy between the data for PILEDRIVER and HARDHAT.

As the energy from the source propagates across the computational model a certain amount of work due to compression is done on the cells of the model. This work, which is essentially $p\,dv$, where p is the pressure and dv is

the volume change, increases the specific internal energy of the cell, therefore increasing its temperature. When the specific internal energy reaches a given value, the material starts to melt. As it was already pointed out before, in this work, the position of this melting point was selected as the criterion used to identify where the boundary of the cavity area is located, i.e., the last melted cell, counted by starting from the center of the source, is located and the coordinate of its center is taken as the final cavity boundary in that area.

In the first stage of this project the evolution of the final cavity size with the depth of burial was investigated with the help of a 1D spherical computational model. A constant overburden pressure, corresponding to the working point depth, was applied to the whole model. The results obtained for the evolution of the final cavity size as a function of the depth of burial are shown in Figure 4.

It is worth noting that Heard's equation for the cavity radius used for the Mueller and Murphy (1971) curve in Figure 4 was

$$r_c = 16.3 W^{0.29} C h^{-0.11} \tag{1}$$

where W is the yield in kilotons, h is the depth of burial in meters and C is a material dependent constant given by

$$C = E^{0.62} \rho^{-0.24} \mu^{-0.67} \tag{2}$$

where E and μ are the Young's and shear moduli respectively and ρ is the material density. In our calculations

$$C = 1.4616 \tag{3}$$

The equation used for the *Denny and Johnson* [1991] curve in Figure 4 was

$$r_c = \frac{14700 W^{1/3}}{\beta^{0.3848} P_0^{0.2625}} \tag{4}$$

where β is the shear wave velocity in meters per second and P_0 is the overburden pressure in Pascal. The numerical values for the material properties used in this paper are given by

$$\begin{aligned} E &= 73.92 \text{ GPa} \\ \rho &= 2680 \text{ kg/m}^3 \end{aligned} \tag{5}$$

The rest of the variables can be derived from these two. The yield was kept constant at one kiloton.

When the shot is done at deeply over buried locations the calculated cavity size is very close to the predictions of Mueller and Murphy (1971). As the depth of burial gets closer to the nominal value, i.e., 125 m for a 1 kiloton source, the calculated final cavity size gets closer to the predictions done by Denny and Johnson (1991).

For the purpose of validation, a comparison of the calculated final cavity sizes for PILEDRIVER and HARDHAT against the measured quantities is presented in Table 1. The calculated values are within 12% of the measured.

The second part of this year's project effort involves the analysis of the cavity size evolution with the depth of burial utilizing a 2D axially symmetric computational model. These 2D simulations are being processed at the time this paper is being prepared. The first results regarding the final cavity size that were obtained from the 2D simulations are confirming the 1D values shown in Figure 4.

As an example of the 2D results, the wave propagation pattern 0.3 s after the shot is shown in Figure 5. The direct P wave resulting from the explosion is shown, followed by the pP wave, which is a result of the bouncing back of the direct P wave against the free surface. The shear pS wave that is generated as a result of the interaction between the free surface and the main wave can also be seen in Figure 5.

The computational model used to simulate the 2D examples presented in this work does not include the possibility of fracturing or spallation inside the rock. In spite of this, a preliminary prediction of the spall areas can still be made with the existing computational tool. Each material has a certain tensile strength that defines when a tensile fracture would start to develop. Tensile stresses are identified by negative pressures in the computational model. In Figure 6 four different snapshots are shown where the spall regions are marked. In this case, the tensile strength of the rock was assumed to be equal to 10 MPa.

Even if the spall areas can be defined, the actual influence of the fracture of the material on the seismic signals is not being properly captured, i.e. an explicit fracture simulation would be necessary to account for this phenomenon. With respect to this matter and as a result of a project that developed over the last years, a state of the art combined finite-discrete element methodology (FEM-DEM) (Munjiza, 2004) was recently implemented within the CASH hydrocode. This new methodology combines the ability of the discrete element method to deal with a large number of interacting particles while keeping the finite volume ability to model the internal deformation of the material. The areas where fracture and/or fragmentation could occur are modeled as a collection of discrete regions or elements connected among them through their common boundaries, giving a continuum like behavior. This connection between the discrete elements is described through the appropriate material fracture variables, i.e. fracture surface energy, maximum normal and tangential displacements, etc. In this way, if the stress state across the discrete element boundaries is such that the fracture toughness of the material is not exceeded, the material behaves as a continuum. However, if the fracture toughness of the material is passed, a transition from continuum to discrete behavior occurs, with a series of fracture patterns as a result. This capability will be very helpful in the future of the project when spallation areas are to be defined, and their effects to be quantified.

One of the main aspects of the simulation of underground explosion is to be able to properly handle extremely high strain rate phenomena. On this matter, the newly implemented FEM-DEM methodology was tested to the extreme, demonstrating that it is up to the challenge (Rougier and Knight, 2010a; Rougier and Knight, 2010b; Rougier et al., 2010a).

CONCLUSIONS AND RECOMMENDATIONS

The source model approaches used in the past arguably do not fully account for the first principle physics of the shock wave continuum from the cavity expansion all the way up to the final energy deposition in the granite elastic region, i.e. there is a gap between the near source region and the near/far field region dynamics. In an effort to try to close this gap the Tillotson EOS was implemented. The verification and validation of this EOS was done by simulating the PILEDRIVER and HARDHAT events. It was shown that the material model developed is in good agreement with the HARDHAT experimental data: velocity and displacement attenuation profiles as well as final cavity radius prediction and expected energy distribution.

This material model was used to predict the behavior of the final cavity size as a function of the depth of burial for a constant yield of one kiloton. The results obtained showed that the locus of the calculated final cavity size is located between the predicted curves of Denny and Johnson (1991) and Mueller and Murphy (1971), as shown in Figure 4. It can be seen from the figure that Denny and Johnson and Heard's curves from Mueller and Murphy have a stronger dependency on the depth of burial than the results obtained from the numerical calculations.

The next steps on the project will be concentrated on the improvement of the current strength model. The main modifications that are planned to be incorporated are: strain softening, strain hardening and high energy effects. A series of sensitivity studies are to be conducted after the improved material model is implemented. These studies will mainly concentrate on the dependence of the final cavity size on the yield of the explosion and on the main material properties (i.e., Poisson ratio, density, "yield surface", etc.) These studies will improve our understanding of the differences between the statistical and calculated hydrocode results.

The capability demonstrated in the present work provides a valuable tool to estimate the characteristics of unknown sources that have been tested on similar materials, like the case of the DPRK test site.

Further studies utilizing the above defined FEM-DEM capabilities coupled with the newly developed equation of state will enable us to reach a new plateau of understanding of how the seismic shear wave generation is affected by the fracture and fragmentation of the material surrounding the source area, and by the spallation of the material located above the working point.

It is worth noting that this new EOS and material model approach combined with the first principles hydrocode will be applied to the National Center for Nuclear Security (NCNS) 2011 studies at the Nevada Test Site (Rougier et al. 2010b).

REFERENCES

Antoun, T. H., I. N. Lomov, and L. A. Glenn (2001). Development and application of a strength and damage model for rock under dynamic loading, *The 38th U.S. Rock Mechanics Symposium*, UCRL-JC-142748.

Denny, M. D. and L. R. Johnson (1991). The explosion seismic source function: models and scaling laws reviewed, *Explosion source phenomenology. Geophysical monograph 65,* American Geophysical Union: 1–24.

Fossum A. F. and R. M. Brannon (2004) THE SANDIA GEOMODEL: Theory and User's Guide. Sandia National Laboratories.

Melosh, H. J. (1989) Impact cratering. A geologic process. *Oxford Monographs on Geology and Geophysics:* 11.

Mueller, R. A. and J. R. Murphy (1971). Seismic characteristics of underground nuclear detonations. Part I. Seismic spectrum scaling, *Bulletin Seismol. Soc. Am.* 61(6): 1675–1692.

Munjiza, A. (2004). The combined finite-discrete element method, *John Wiley & Sons.*

Rimer, N., J. Stevens, and D. Halda (1990). Modeling of the ground motion from events in genetic rocks, *Modeling and Material Properties Working Group of the CAT,* SSS-DVR-90-11661.

Rougier, E., and E. E. Knight (2010a). Slidelines in CASH. Benchmark Tests and Practical Applications. Los Alamos National Laboratory, LA-UR-10-00908.

Rougier, E., and E. E. Knight (2010b). Fracture in CASH - Benchmark Tests and Practical Applications. Los Alamos National Laboratory, LA-UR-10-03254.

Rougier, E., A. Munjiza, C. Bradley, T. Carney, E. E. Knight, and W. M. Brunish (2010a). Geodynamics and geomechanical analysis using combined finite element and discrete element modeling. Los Alamos National Laboratory, LA-UR-10-04033

Rougier, E., E. E. Knight, and W. M. Brunish (2010b). Source Physics Experiments. HANFO Ground Shock Estimates. Los Alamos National Laboratory, LA-UR-10-04449.

Schroeder, R. C. (1974). A comparison of initial conditions for nuclear explosion calculations, UCRL-51671.

Tillotson, J. H. (1962). Metallic equation of state for hypervelocity impact, AF 29(601)-4759, ARPA Order 251-61.

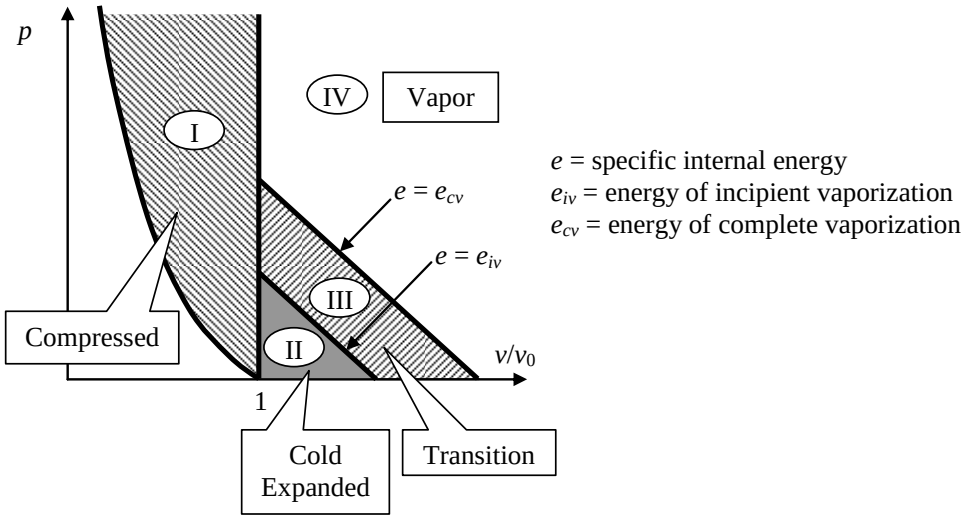

Figure 1. Tillotson EOS. Different phases in the p-v plane. - Phase I: Compressed states for all values of e. Phase II: Expanded state with $e < e_{iv}$. Phase III: Expanded state with partial vaporization $e_{iv} < e < e_{cv}$. Phase IV: Expanded state with complete vaporization $e_{cv} < e$.

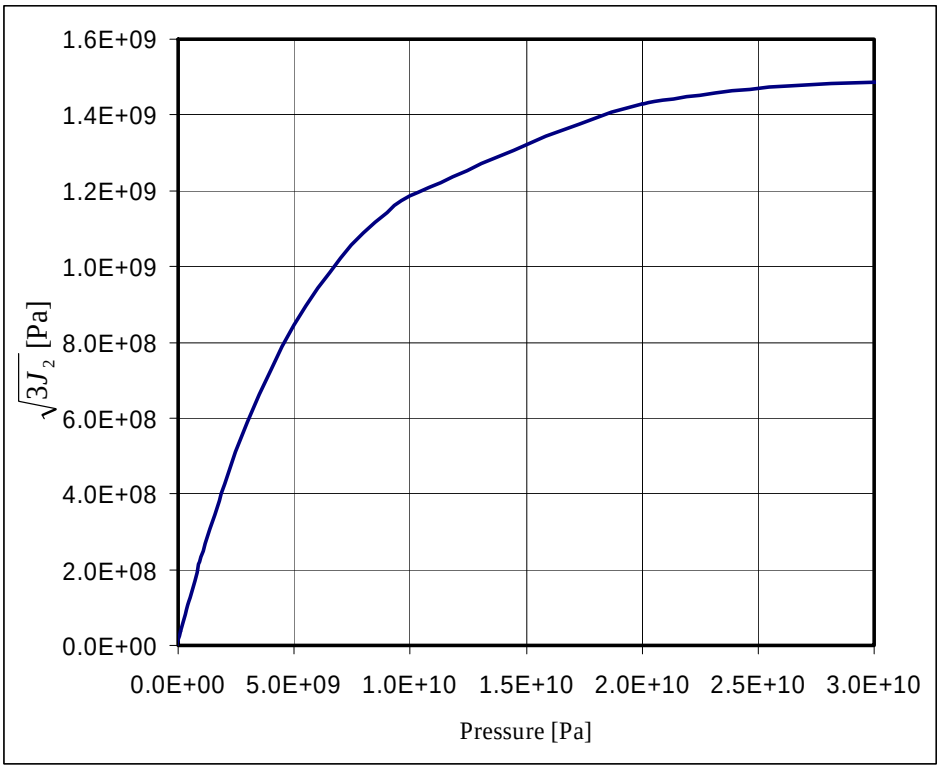

Figure 2. Yield surface used in the simulations presented in the current work.

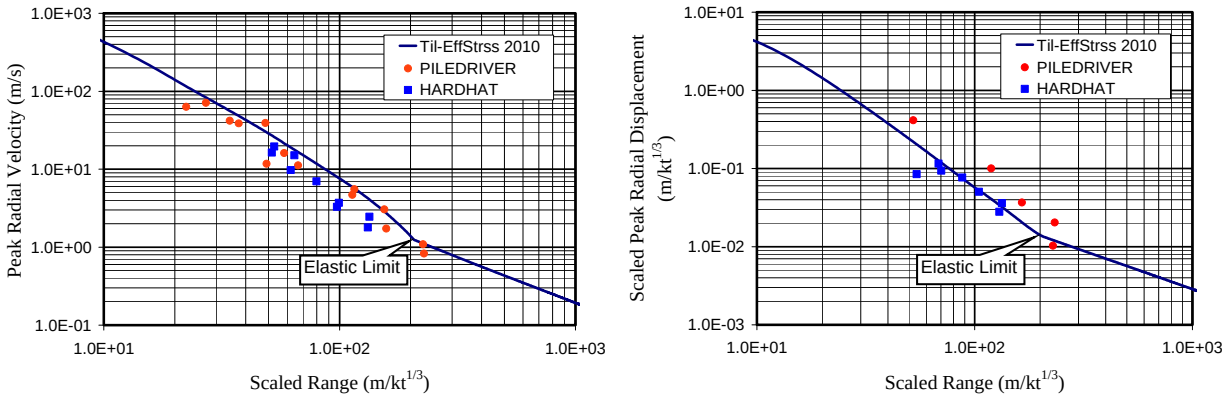

Figure 3. Material model validation: Peak radial velocity (left) and scaled peak radial displacement (right) as a function of the scaled range.

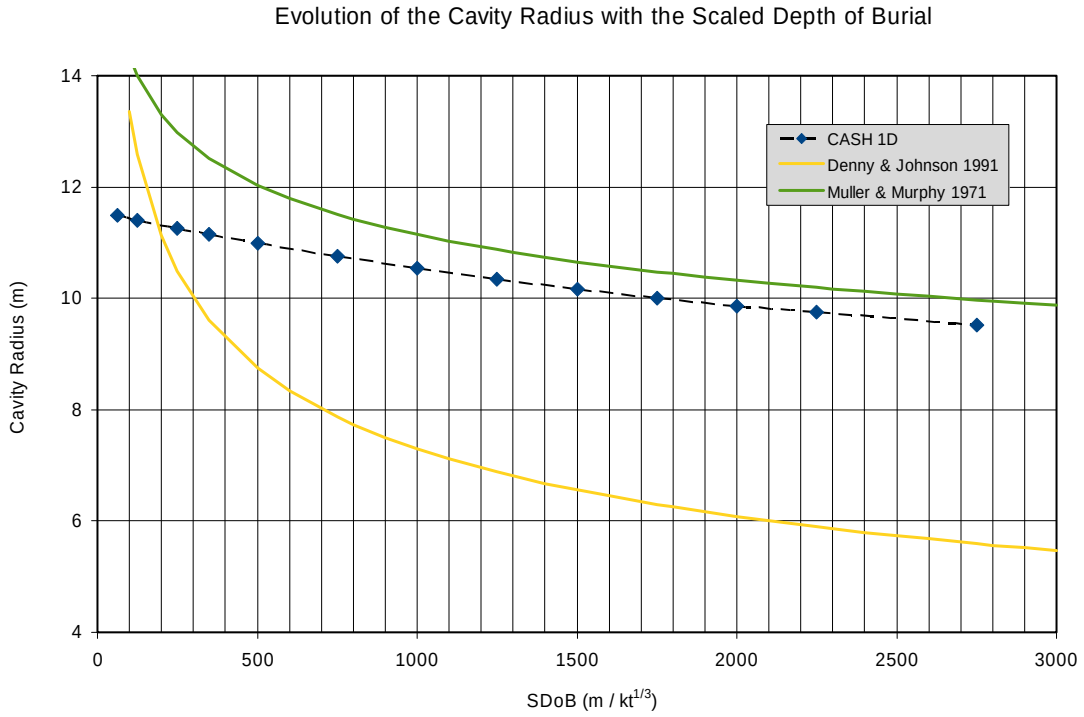

Figure 4. Evolution of the cavity size with the scaled depth of burial. Graphs constructed for a constant yield of 1 kiloton.

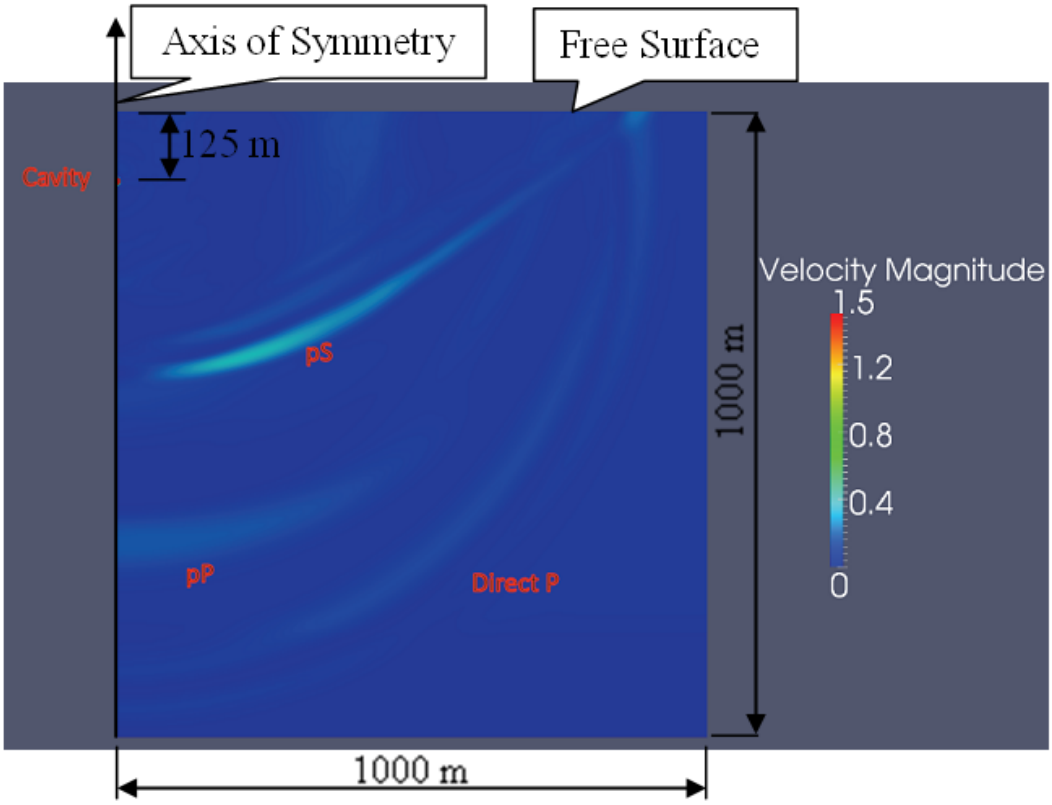

Figure 5. Velocity profile for a 1kt charge buried at nominal DoB (125 m) taken 0.3 sec after the shot.

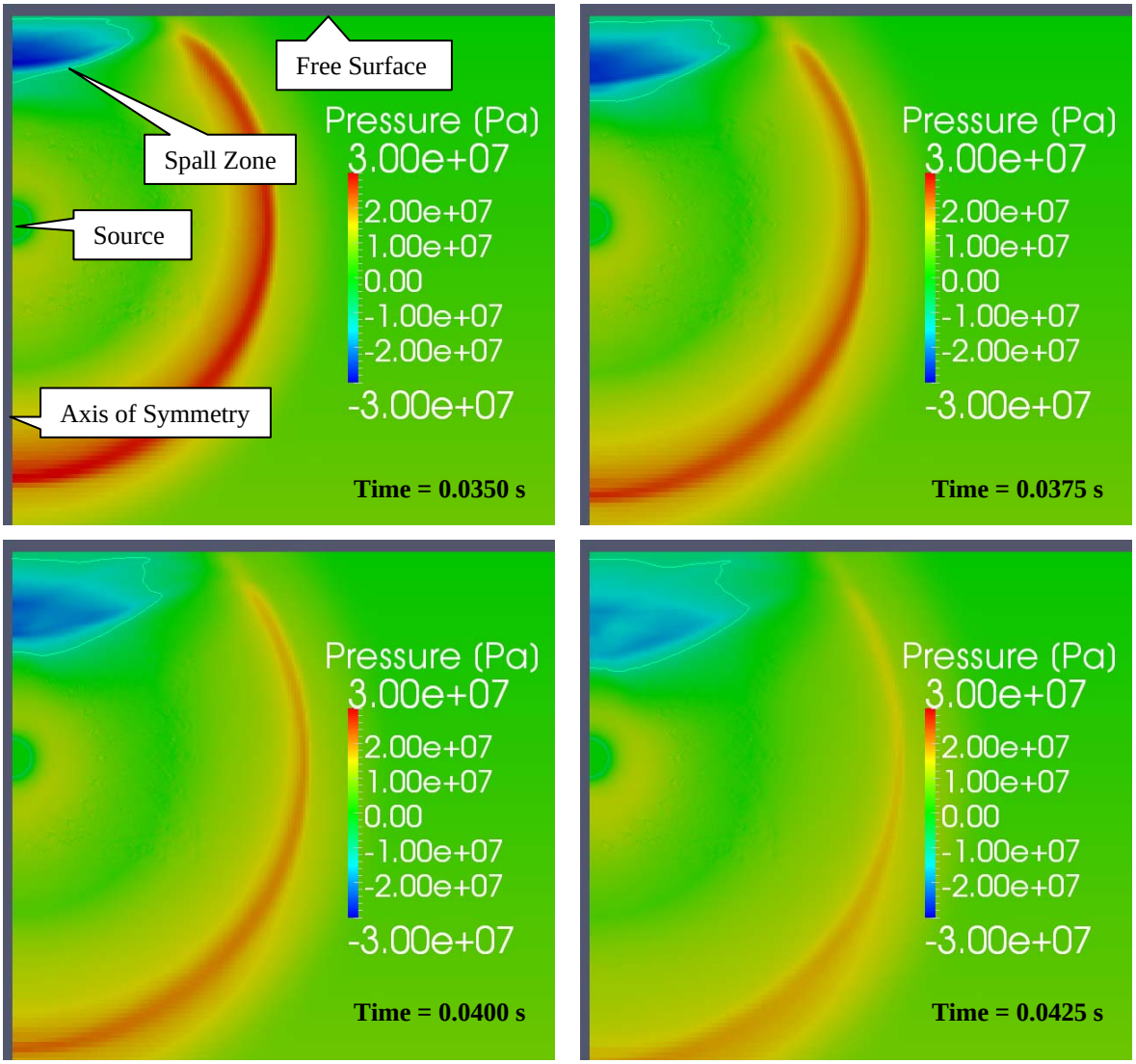

Figure 6. Prediction of the spall zone for a 1kt charge buried at nominal DoB (125 m).

Table 1. Comparison of measured and calculated final cavity radius.

	PILEDRIVER	HARDHAT
Measured Final Cavity Radius (m)	44.5	19.4
Calculated Final Cavity Radius (m)	42.7	21.8